RSC Advances

PAPER

View Article Online
View Journal | View Issue

Cite this: *RSC Adv.*, 2019, **9**, 8326

Generation of engineered core–shell antibiotic nanoparticles†‡

Kokkarachedu Varaprasad, *[a] Murali Mohan Yallapu,[b] Dariela Núñez,[a] Patricio Oyarzún,[c] Matias López,[ac] Tippabattini Jayaramudu[d] and Chandrasekaran Karthikeyan[e]

Well-defined nanocomposite structures have received significant attention due to their superior combinatorial properties. Rational tuning of the core and shell of the nanostructure(s) can offer potent antibacterial activity. Such advanced core–shell nanocomposite methodologies allow not only the incorporation of antibacterial agents on the shell but also provide its stability and nurture antibacterial activity. Herein, antibiotic zinc oxide–curcumin (ZnO–Cum) core–shell nanoparticles for antibacterial application were synthesised. The ZnO–Cum core–shell nanoparticles were prepared by curcumin nanolayer deposition on zinc oxide nanoparticles *via* a sonication process. The resulting ZnO–Cum core–shell nanoparticles were spiracle in shape with a ~45 nm ZnO core and ~12 nm curcumin shell layer size, respectively, determined by transmission electron microscopy. X-ray diffraction analysis confirmed the formation of a core–shell crystal structure. Additionally, UV-DRS and ATR-FTIR spectral analysis support the existence of ZnO and curcumin in a core–shell nanocomposite. The antibacterial activities of nanoparticles developed were studied against *Staphylococcus aureus and Streptococcus pneumoniae* and *Escherichia coli* and *Shigella dysenteriae* bacterial stains using the diffusion method. A greater inhibition of the growth of Gram positive and negative bacteria was noticed upon treatment with core–shell ZnO and curcumin nanoparticles than the commercial antibiotic amoxicillin which indicates their antibacterial property. The findings of this study provide evidence that the zinc oxide–curcumin core–shell nanoparticles may be highly promising for antibacterial and biomedical applications.

Received 21st January 2019
Accepted 6th March 2019

DOI: 10.1039/c9ra00536f

rsc.li/rsc-advances

Introduction

Engineered nanoparticles have attracted much attention and interest as antibiotics to improve the quality of human life, due to their advanced physical, chemical, and biological characteristics. Principally, antibiotics are often composed of inorganic or organic materials.[1] These antibiotic materials have been proposed in biomedical applications for the treatment of pneumonia, bloodstream infections, kidney failure, urinary tract infections and mainly wound infection treatments. Overall, antibiotics are used for curing human and animal diseases in clinical applications.[2] Lately, a wide range of inorganic and organic materials have been used for the preparation of antibacterial nanocomposite materials (antibiotics). According to green chemistry, antibiotic inorganic nanoparticles were developed using several methods.[3] Among them, the precipitation method is simple, cost-effective and makes it easy to regulate the morphology of inorganic nanomaterials.[3,4] In the case of hydrophobic organic materials, the ultra-sonication process is more simple and effective for the formulation of nanoparticles to get better dissolution with pharmacokinetic properties.[5,6]

Zinc oxide is one of the non-toxic, biocompatible and inexpensive inorganic antibiotic materials.[7] It shows significant antibacterial activities against bacteria, fungus and virus.[8] Therefore, it is an important compound for biomedical industries.[7] However, many researchers presented reports that showed that the ZnO can show low toxicity on the human, plants and animals cells.[8,9] Lately, to reduce the toxicity of the antibacterial ZnO nanoparticles and to enhance its applicability in biomedical, it was prepared as an antibiotic nanocomposite with several kinds of organic and inorganic materials.[8,10] However, the toxicity of the materials depends on the composition of the materials.[8,10]

[a]*Centro de Investigación de Polímeros Avanzados, CIPA, Edificio de Laboratorios, Avenida Collao 1202, Concepción, Bio-Bio, Chile. E-mail: varmaindian@gmail.com; prasad@cipachile.cl*

[b]*Department of Pharmaceutical Sciences and Center for Cancer Research, University of Tennessee Health Science Center, Memphis, TN 38105, USA*

[c]*Facultad de Ingeniería y Tecnología, Universidad San Sebastián, Lientur 1457, Concepción, Chile*

[d]*Laboratory of Material Sciences, Instituto de Quimica de Recursos Naturales, Universidad de Talca, Talca, Chile*

[e]*Kind Institute of Research and Development Pvt Ltd, Trichy, Tamilnadu-620020, India*

† Presented in Biomaterials-7th EuCheMS Chemistry Congress.

‡ Electronic supplementary information (ESI) available. See DOI: 10.1039/c9ra00536f

Curcumin (1,7-bis-{3-methoxy-4-hydroxyphenyl}-1,6-heptadiene-3,5-dione) is one of the nontoxic, hydrophobic, polyphenolic compound which is an extract from turmeric (*Curcuma longa*) and has low solubility in aqueous media.[11] To overcome this problem, various methods are developed for enhancing its applicability in the biomedical field. Among them, an ultra-sonication process is more efficient at the nanocurcumin formulations.[12] It has potent anti-oxidative, anti-inflammatory, antimicrobial, antitumor, anti-HIV and anti-carcinogenic properties.[5,13–15] In addition, curcumin reduces the toxicity of complex materials and inhibits singlet oxygen, nitric oxide, superoxide anion, lipid peroxidation and hydroxyl radicals.[15,16] Therefore, it has been used for clinical and food applications.[14] Conversely, curcumin can form a potent complex with organic and inorganic materials and offer innovative physicochemical and medical properties.[5,17,18] Especially it formed a complex with ZnO, 3-mercaptopropionic acid and their derivative materials *via* conjugation process.[19] The resulted conjugate product was used for cancer treatment. Simply complex nanocomposites were used for removal of arsenic from polluted water.[20] Besides, it is used as a reducing and stabilizing agent for inorganic particles.[18]

Herein, employing an ultra-sonication process, it synthesized antibiotic core–shell nanocomposites from organic curcumin and inorganic zinc oxide. To the best of our knowledge, this is the new report on antibiotic core (ZnO)–shell (curcumin) nanocomposites. In this investigation, the required ZnO was developed *via* a simple precipitation method. Advantages of these economical methods are simple and facile preparation of antibiotic nanoparticles. The resulted nanomaterials were characterized by XRD, FTIR, UV/DRS, SEM/EDS, and TGA/DSC. A typical bacterium, *Staphylococcus aureus*, *Streptococcus pneumoniae*, *Escherichia coli* and *Shigella dysenteriae* were used to evaluate the antibacterial activity of the antibiotic nanomaterials.

Results and discussion

In this investigation, the ultra-sonication technique was employed to develop the antibiotic nano-curcumin, ZnO_x/Cum $\times 1$ (x = 0.375, 0.25, 0.125, $\times 1$ = 0.125, 0.25, 0.375) core/shell nanoparticles, and simple precipitation method was used to develop the ZnO nanoparticles. The XRD patterns of developed antibiotic nanoparticles are shown in Fig. 1. XRD data analysis of the nano-curcumin showed well-developed crystalline peaks.[21,22] The main characteristic peaks of nanocurcumin appeared at diffraction angles of 2θ at 12.09, 14.62 and 17.29° indicating that nanocurcumin stays existent as a crystalline form.[21,22] The XRD pattern of ZnO shows the diffraction peaks of crystalline ZnO in the hexagonal wurtzite structure. The peaks have been identified as JCPDS card no. 36-1451 by WinXPow software.[4] Similarly, $ZnO_{0.25}$–$Cum_{0.25}$ and $ZnO_{0.125}$–$Cum_{0.375}$ show strong curcumin and ZnO peaks.

ATR-FTIR spectroscopy is a valuable tool that indicates the combined interaction of nanocurcumin and ZnO nanoparticles (Fig. 2A and B). For curcumin, bands observed at 3504.91 (phenolic OH), 1620.99 (C=C & C–O), 1503.15 (C=O), 1433.52, 1265.94 (enol C–O), 1143.51 (C–O–C), 956.03 (benzoate *trans*-CH) and 804.52 cm^{-1} (C–H) are corresponding to the functional groups (phenolic OH, C–O, C=C, C–O–C) of curcumin.[23] Similarly, the nanocurcumin spectrum showed similar functional groups without any changes in the band positions. For ZnO, the peaks observed at 415 and 666.79 cm^{-1} corresponding to Zn–O stretching mode.[24] The of core/shells nanocomposites, ZnO stretching mode was observed at 405 cm^{-1} and it was observed that when the ZnO content in the nanoparticles composition was increased, the percentage of transmittance was changed which is due to ZnO transparency and its strong (π–π) interaction with curcumin.

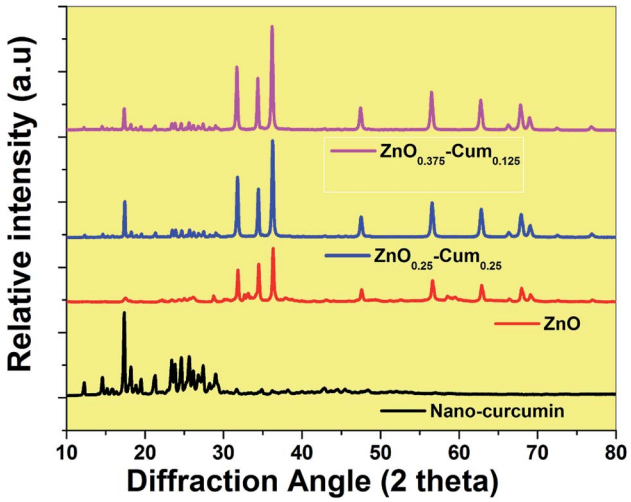

Fig. 1 XRD spectra of the nanomaterials.

To further characterize the nanoparticles, the melting temperatures of the curcumin nanoparticles were measured by using the DSC (Fig. 2C and D). The DSC curves of the curcumin, nano-curcumin, $ZnO_{0.375}$–$Cum_{0.125}$, $ZnO_{0.25}$–$Cum_{0.25}$, and $ZnO_{0.125}$–$Cum_{0.375}$ are presented in Fig. 2C and D. The curcumin exhibited endothermic melting temperature (T_m) at 190.10 whereas nano-curcumin exhibited endothermic T_m at 191.10 which can occur because of the high crystalline nature of nanomaterials.[21] However, an increase in the melting peaks of core/shell incorporated ZnO was observed. The increasing order was as follows: $ZnO_{0.375}$–$Cum_{0.25}$ > $ZnO_{0.25}$–$Cum_{0.25}$ > $ZnO_{0.125}$–$Cum_{0.375}$. Here, T_m of the nanocomposites is mainly depending on ZnO and curcumin content. Sun *et al.* have reported material's thermal stability depending on their physical mixtures of the composite materials.[25]

The thermal properties of the nanomaterials were investigated by using a TGA analysis under a nitrogen atmosphere (Fig. 3). The results explained that the developed core–shell nanoparticles have a hydrophobic nature which came from curcumin.[26] Therefore, nanomaterials did not exhibit any stage of water molecules loss in the TGA curves. Similarly, hydrophobic curcumin and nano-curcumin have not shown water molecule weight loss in the TGA analysis.[25] Here, ZnO's first weight loss arises at 50–70 °C due to evaporation of water molecules and curcumin free material.[24] All nanomaterials exhibited their initial weight loss at 190–210 °C, which is due to dihydroxylation of OH groups of curcumin molecules decomposition.[27] However, the final

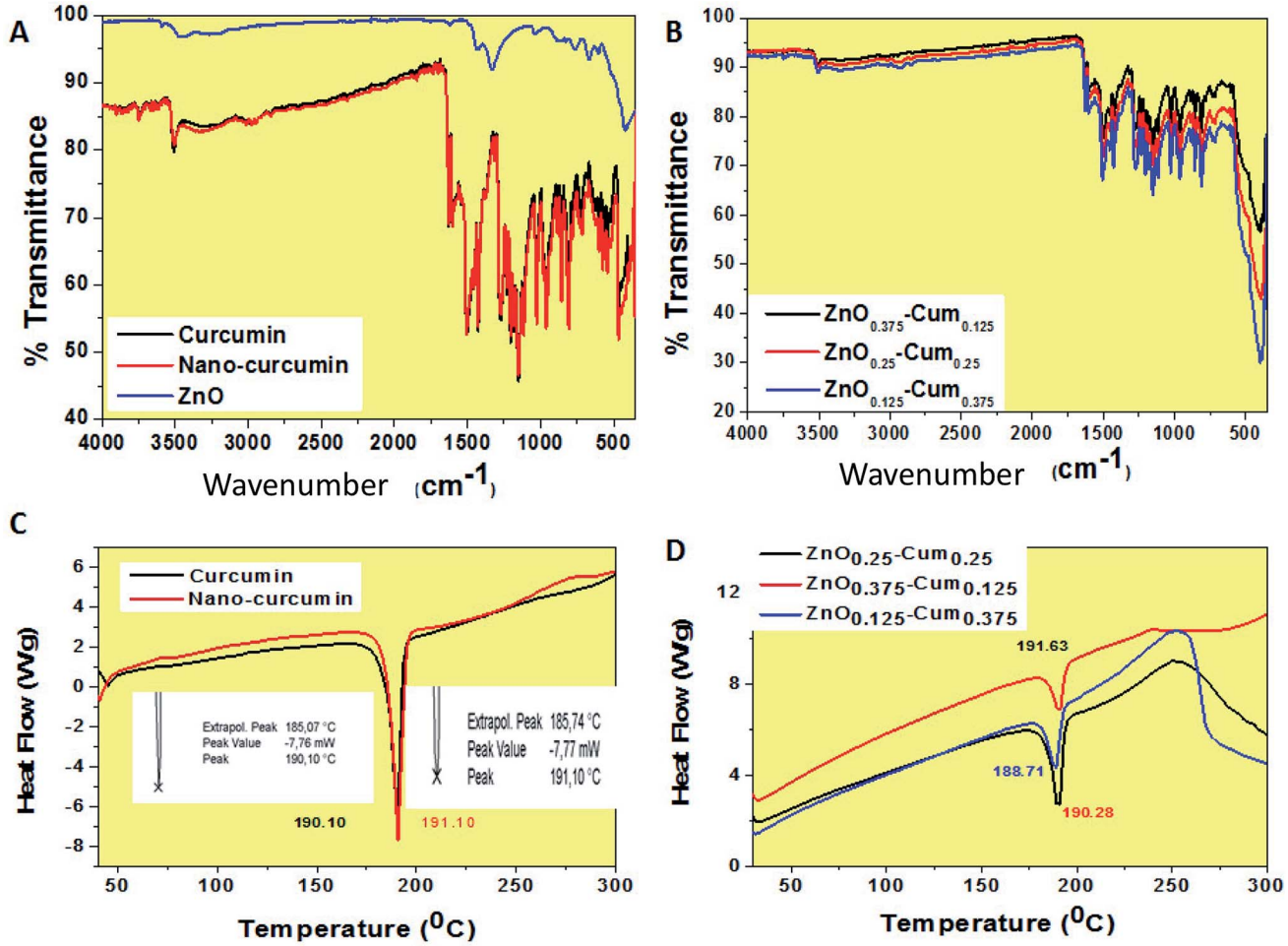

Fig. 2 ATR-FTIR and DSC spectra of the (A & C) pure curcumin, nanocurcumin and ZnO and (B & D) $ZnO_{0.375}$–$Cum_{0.125}$, $ZnO_{0.25}$–$Cum_{0.25}$ and $ZnO_{0.125}$–$Cum_{0.375}$ core–shell nanoparticles.

weight losses of curcumin, nano-curcumin, ZnO, $ZnO_{0.375}$–$Cum_{0.125}$, $ZnO_{0.25}$–$Cum_{0.25}$, and $ZnO_{0.125}$–$Cum_{0.375}$ were observed at 750 °C are 73.55, 66.64, 28.61, 41.2, 43.4 and 51.88% respectively. In the weight loss comparison of $ZnO_{0.125}$–$Cum_{0.375}$ to the $ZnO_{0.25}$–$Cum_{0.25}$, the $ZnO_{0.375}$–$Cum_{0.125}$ enhanced the weight loss of material. The result suggests that increasing the ZnO nanoparticles in the core–shell, the weight loss of nanomaterials decreases due to strong physical interaction at the interface face of ZnO/curcumin. And also the result suggests that the developed nanocurcumin has higher thermal stability than the curcumin due to the crystalline nature of the nanocurcumin.[28] Overall, the ZnO has exhibited a low rate of weight loss and it can improve the thermal properties of the core–shell nanoparticles and curcumin can improve the hydrophobic nature of the core–shell.

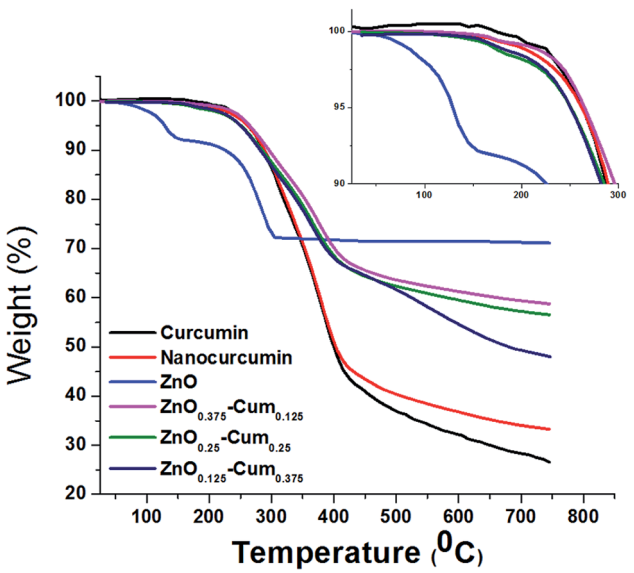

Fig. 3 TGA curves of pure curcumin and developed nanomaterials.

SEM/EDS studies were carried out to obtain the nanostructure/morphology and elemental concentration of nanomaterials developed. Fig. 4 shows the SEM images of nanocurcumin, ZnO and its nanocomposite materials. The SEM micrographs reveal that each sample shows different morphology. EDS analysis confirmed the dispersion of the ZnO nanoparticles in the nanocurcumin and they showed C, Zn and O elements. However, when the ZnO content in the nanocomposite is increased, an increment of Zn element was found in the EDS analyses. Similarly, increasing the curcumin content in the nanocomposite increased the C element.

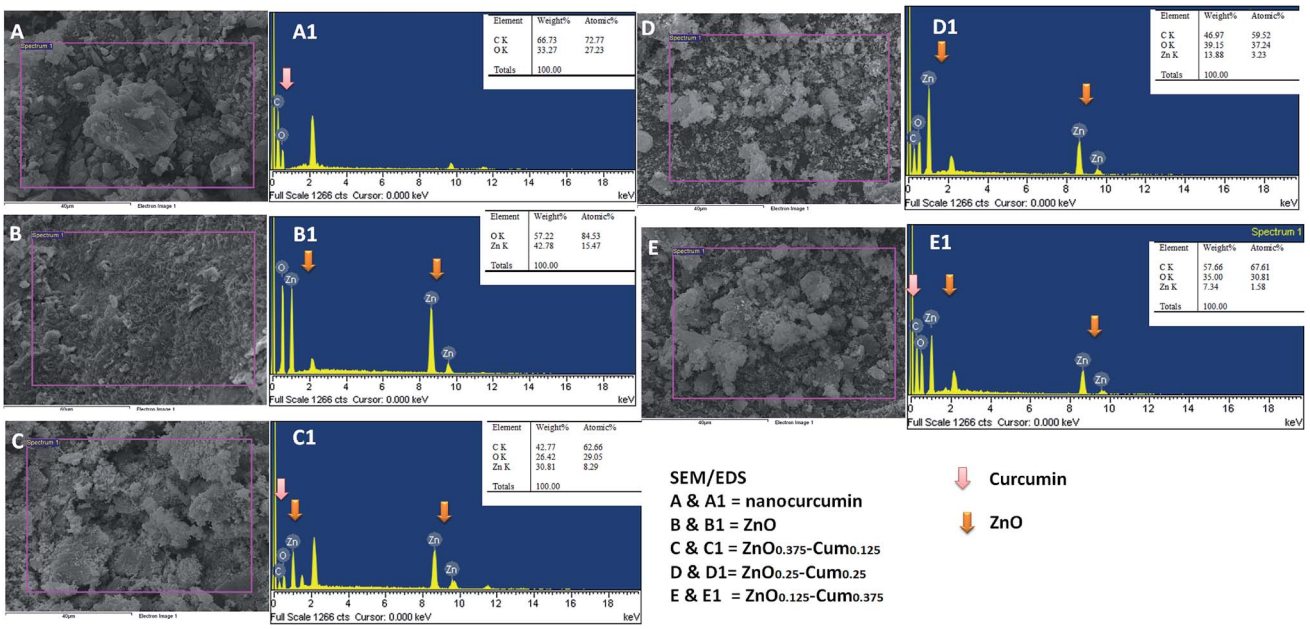

Fig. 4 SEM/EDS images of nanomaterials.

The typical morphology of the nanocomposites is shown in Fig. 5. The TEM micrographs attest that the chosen process has resulted in completing the sonication process by growing shape tuned size nanoparticles ranging around ~57 nm. Fig. 5B ($ZnO_{0.25}$–$Cum_{0.25}$) shows the clear image of curcumin as a shell and ZnO as a core. Resulted ZnO–Cum core–shell nanoparticles are spiracle in shape with ~45 nm ZnO as a core and ~12 nm curcumin as a shell layer size, respectively determined by transmission electron microscopy. Fig. 5D shows the UV-vis diffused reflectance spectra of the developed nanoparticles and nanocomposites. The results explained that ZnO, curcumin and nanocurcumin exhibited their absorption bands at ~365 nm, ~471 nm, and ~471 nm, respectively.[29,30] In all nanocomposites, curcumin and ZnO peaks were observed at ~451 nm and ~353 nm respectively. Here, the absorption peak intensity changes with curcumin and ZnO content in the nanocomposites. However, this phenomena depends on the π–π* electronic transition of nanomaterials.[29] Ghaffari *et al.* has obtained similar phenomena in the ZnO–MPA–curcumin nanoformula.[19] The band gap values for the nanomaterials were calculated using the Planck's formula equation.[3] Equation is $E_{bg} = \frac{hc}{\lambda} = \frac{1243.1}{\lambda}$ (eV) where E_{bg} is the band-gap energy (eV), h is the Planck's constant ($4.135\,667 \times 10^{-15}$ eV s) and λ is the wavelength (nm) of the nanomaterials. The band gaps of curcumin, nanocucumin and ZnO are found to be ~2.6 eV, ~2.6 eV and ~3.40 eV respectively. Due to the wide band gaps of ZnO, it cannot absorb any visible light in the visible region[31] whereas all core–shell ($ZnO_{0.375}$–

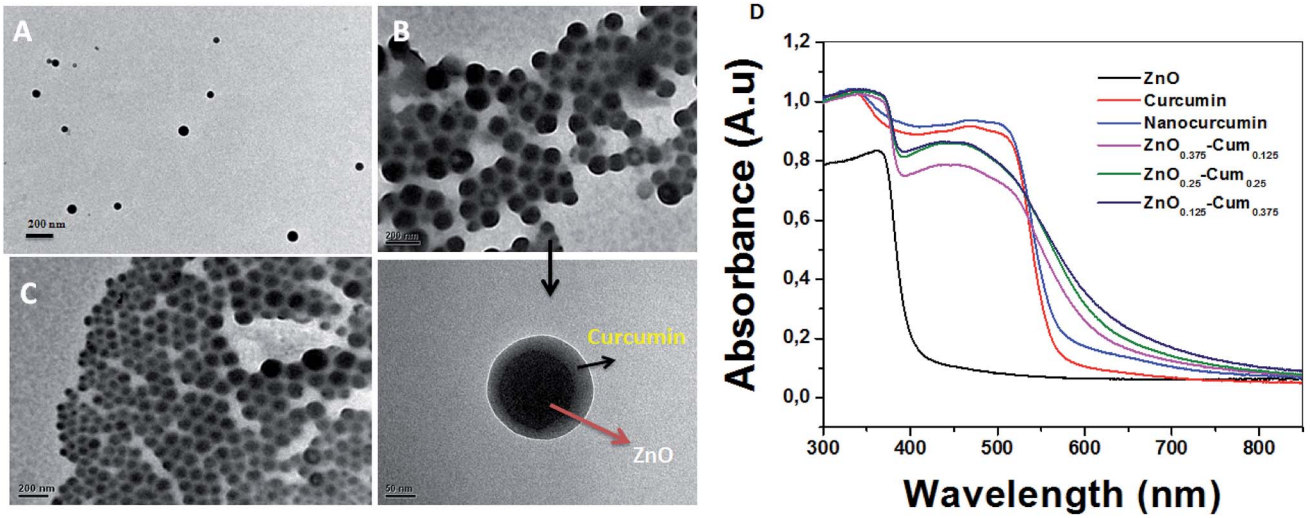

Fig. 5 TEM images of (A) $ZnO_{0.375}$–$Cum_{0.125}$, (B) $ZnO_{0.25}$–$Cum_{0.25}$ and (C) $ZnO_{0.125}$–$Cum_{0.375}$ nanomaterials and (D) UV-DRS spectra of pure curcumin and nanomaterials.

$Cum_{0.125}$, $ZnO_{0.25}$–$Cum_{0.25}$, and $ZnO_{0.125}$–$Cum_{0.375}$) nanomaterials were shown same of band gaps (curcumin ~2.75 eV and ZnO ~3.52 eV) values of their composition. Due to curcumin, core–shell nanoparticles were observed the visible light in the range of 200–550 nm. Similarly, the reflectance spectra (ESI data S2†) of nanomaterials showed similar information. However, this kind of hydrophobic core/shell materials could be useful to protect human skin from ultraviolet A (320–400 nm), B (280–320 nm) and C (200–290 nm) light.[32,33]

Furthermore, it was observed that the curcumin is poorly soluble (ESI data S3†) in aqueous media, due to its hydrophobic chemical nature and surface areas.[16] Whereas developed nanocurcumin, nanocomposites were fully dispersible in aqueous media due to its high surface areas of nanomaterials.[16] And also observed that ZnO–Cum (core–shell) nanocomposites have better water solubility than other materials. The similar report was observed in the literature.[34] This kind of phenomenon will enhance their applicability in biomedical applications. ESI data S4† shows the absorption spectra of the aqueous solution of curcumin, nanocurcumin, ZnO, and nanocomposites in the spectral region of between 350 nm and 600 nm. The absorption band at 374 nm indicated the formation of ZnO NPs by precipitation method.[35] However, curcumin and nanocurcumin showed a wide-range narrow absorption which indicates the characteristic absorption of the curcumin, similar kind of phenomena was obtained in the previous report.[23] Similarly, when ZnO content is increased in the core/shell composition, the UV absorption is decreased.

The antibacterial activities of developed nanomaterials were tested against *Staphylococcus aureus, Streptococcus pneumoniae*, *Escherichia coli* and *Shigella dysenteriae* bacteria by disk diffusion method (Fig. 6A–D). The selected bacteria caused serious infection to the human system such as breathing problems, dysentery, anaemia or kidney failure, wound infections and urinary tract infections. The zone of inhibition results explains that selected samples exhibited good antibacterial activity than commercial antibiotic amoxicillin and when the ZnO content in the core–shells is increased, the zone of inhibition increased (Fig. 6E) whereas pure zinc oxide showed the highest antibacterial activity among nanomaterials. This is due to the generation of reactive oxygen species and the release of Zn^{2+} from ZnO, bacteria losing the viability of cell division and finely bacterial cells death occurs.[36,37] Teng ng *et al.* has clearly stated that the toxicity of the ZnO (on bacteria) depends on several factors.[38]

The generation of highly reactive species (OH^-, H_2O_2 and $^{\bullet}O_2^-$) mechanism is explained as follows. Since ZnO with defects can be activated by both UV and visible light; electron–hole pairs (e^-, h^+) can be created. The holes split water molecules (from the suspension of ZnO) into OH^- and H^+. Dissolved oxygen molecules are transformed to superoxide radical anions ($^{\bullet}O_2^-$), which in turn react with H^+ to generate ($HO_2^{\bullet}$), which upon subsequent collision with electrons produce hydrogen peroxide anions (HO_2^-). They then react with hydrogen ions to produce molecules of H_2O_2. The generated H_2O_2 can penetrate the cell membrane and kill the bacteria. The above mechanism of the light-induced generation of ROS can be given in equation form as the following:

$$ZnO + h\upsilon \rightarrow e^- + h^+$$

$$h^+ + H_2O \rightarrow {}^{\bullet}OH + H^+$$

$$e^- + O_2 \rightarrow {}^{\bullet}O_2^-$$

$$^{\bullet}O_2^- + H^+ \rightarrow HO_2^{\bullet}$$

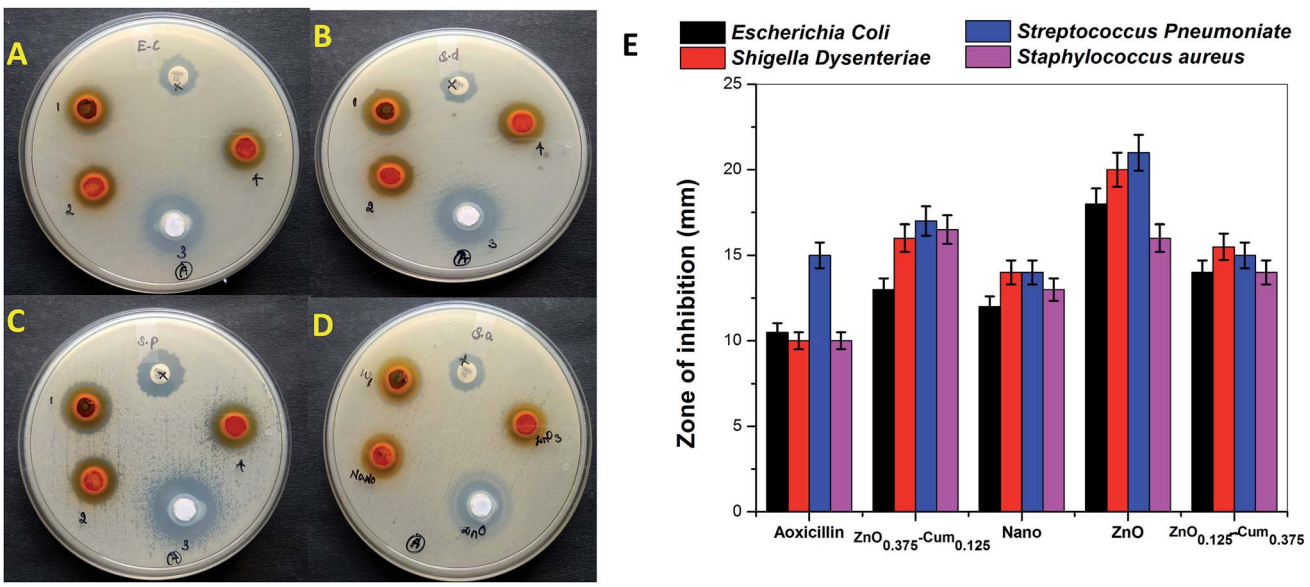

Fig. 6 (A–D) Antibacterial activity of the selected samples. (E) The zone of inhibition formed around each disc, loaded with selected test sample indicated the anti-racial activity of (A) *Escherichia coli* (B) *Shigella dysenteriae* (C) *Streptococcus pneumoniae* and (D) *Staphylococcus aureus* for the $ZnO_{0.375}$–$Cum_{0.125}$ (1 or Zn1) nanocurcumin (2 or nano), ZnO (3), $ZnO_{0.125}$–$Cum_{0.375}$ (4 or ZnO_3) and commercial antibiotic amoxicillin (AMX 10) samples.

$$HO_2^{\cdot} + H^+ \rightarrow H_2O_2$$

The antibacterial efficiency of ZnO NPs generally depends on the presence of more ROS, which is mainly attributed to an increase in oxygen vacancies, the diffusion ability of the reactant molecules and the release of Zn^{2+}.

However, it was observed that curcumin captured nanoparticles having low antibacterial activity than ZnO and higher activity than nanocurcumin. According to the literature, curcumin reduces the antibacterial activity of the metals due to reversible electron transfer reactions with superoxides (molecular oxygen) ions.[39] Similarly, when increasing the curcumin concentration in the core–shell, the generation of superoxide's ions are decreased which reduce the inhibition zone of core–shells. However, when the ZnO content in the core–shells nanoparticles is increased, they showed a good zone of inhibition on Gram-positive and negative bacteria. From, these studies, it was concluded that curcumin and ZnO based nanocomposite materials are highly useful for clinical applications to improve the quality of human life in the 21st century.

Materials and methods

Curcumin (100%), dichloromethane (99.80%), zinc nitrate (99.0%) and ammonium hydroxide (28% NH_3 in H_2O, 99.99%) were purchased from Sigma Aldrich, Chile and used as received.

Preparation of curcumin nanoparticles

Curcumin nanoparticles were prepared over ultra-sonication technique.[28] In this method, curcumin was suspended in dichloromethane (0.5 w/v%) and diffused dropwise into 50 mL steaming distilled water (~100 °C) at a flow rate of 0.2 mL min^{-1} following ultrasonic conditions (power 100 W/frequency 30 kHz). After 15 minutes of sonication, the reaction mixture was stirred at 300 rpm at ambient temperature for 20 minutes till all the organic solvent was evaporated. The clear orange coloured suspension was ultra-centrifuged for 5 min at 4 °C at 12 000 rpm and freeze-dried to obtain nanocurcumin.

Preparation of zinc oxide (ZnO) nanoparticles

ZnO nanoparticles were synthesized by a precipitation technique.[24] Briefly, 0.05 M of $Zn(NO_3)_2$ was dissolved in 50 mL of distilled water under the constant stirring condition at 300 rpm with the ultrasonic condition (power 100 W/frequency 30 kHz) at 21 ± 2 °C for 15 minutes. To this solution, 50 mL of 0.1 M NH_4OH was slowly added dropwise until a white precipitate was formed during which the pH was adjusted to ~9. After 30 minutes of stirring, the resulting solution was washed several times with distilled water and methanol in order to remove the unwanted elements. Finally, precipitation was filtered and dried at 120 °C for 2 h.

Preparation of zinc oxide–curcumin core–shell nanoparticles

Core/shell nanoparticles were prepared by the ultra-sonication method. For the preparation of core/shell, different concentration of curcumin was initially dissolved in dichloromethane to the preparation of three different core/shell nanoparticles (Table 1). Then, the curcumin solution was added to a different concentration of boiling ZnO solution (~100 °C) with a flow of 0.2 mL min^{-1} under ultrasonic conditions (ultrasonic power of 100 W with frequency 30 kHz). After sonication, the reaction mixture was stirred for 30 minutes to evaporate dichloromethane. The resulted solution was ultra-centrifuged for 10 minutes at 4 °C. Then dried to obtain ZnO encapsulated nanoparticles (ESI data S1†).

Table 1 Feed composition of nanomaterials

Nanomaterial code	ZnO (g)	Curcumin (g)
$ZnO_{0.375}$–$Cum_{0.125}$	0.375	0.125
$ZnO_{0.25}$–$Cum_{0.25}$	0.25	0.25
$ZnO_{0.125}$–$Cum_{0.375}$	0.125	0.375

Characterizations

ATR-FTIR spectra of the curcumin, ZnO, and core–shell nanoparticles were obtained from a Perkin Elmer, UATR two, ATR-FTIR spectrometer (Beaconsfield, Bucks, UK) in the wavelength range of 4000 to 400 cm^{-1}. Ultraviolet-visible diffused reflectance spectroscopy (UV/DRS) measurements of nanoparticles were recorded using V760 Jasco spectrophotometer with $BaSO_4$ as a reflectance standard. X-ray diffraction profiles of nanoparticles were studied with Rigaku diffractometer with Cu-Kα radiation for 2θ value range from 10 to 80° at a voltage of 40 kV, a current of 40 mA, and a scan rate of 0.02° s^{-1}. SEM/EDS of curcumin and core/shell nanoparticles were captured by using SEM model JEOL 6460LV. Thermal characteristics of the samples developed were determined on a thermogravimetric analyzer (TGA), using the TGA Q50 T.A instrument-water LLC, Newcastle, DE, USA, at a heating rate of 10 °C min, passing nitrogen gas at a flow rate of 100 mL min^{-1} in the temperature range of 25–600 °C. DSC thermograms of nanoparticles were recorded using a DSC 882e, Mettler Toledo instrument at a heating rate of 5 °C min under a constant nitrogen flow (100 mL min^{-1}) in the temperature range of between 25 °C and 300 °C. Transmission electron microscopy (TEM) images of developed nanoparticles were obtained by TEM model FEI Technai G2 20S-TWIN, USA. For this observation, the core/shell nanoparticles were dispersed in the distilled water and deposited on a 3 mm copper grid and dried at ambient temperature.

Antibacterial activity

The antibacterial activity of nanocurcumin, ZnO, $ZnO_{0.375}$–$Cum_{0.125}$, and $ZnO_{0.125}$–$Cum_{0.375}$ were studied against Gram-positive (*Staphylococcus aureus* and *Streptococcus pneumoniae*) and Gram-negative (*Escherichia coli* and *Shigella dysenteriae*) bacterial stains using the well diffusion method. Petri plates were prepared with 25 mL of sterile Muller Hinton agar media and each bacterial pathogen was individually swabbed on Muller Hinton agar media in separate plates. The antibacterial activity was tested at a concentration of 2 mg mL^{-1} with the required quantity of selected samples dispersed in dimethyl

sulphoxide. The zone of inhibition levels was measured after 24 h, it was incubated overnight at 37 °C. Here, the standard antibiotic amoxicillin (2 mg mL^{-1}) was used as positive control.

Conclusion

An innovative curcumin and zinc oxide-based core (ZnO)–shell (curcumin) nanoparticles were successfully prepared *via* the ultra-sonication process. The resulted nanoparticles were completely characterized. The morphology of developed core–shell structures *w* confirmed by TEM. The nanomaterials showed good solubility in the distilled water. The antibacterial study confirmed that core–shell nanoparticles and nanoparticles performed a better antibacterial activity than the commercial antibiotic amoxicillin. And also confirmed that curcumin modified the antibacterial capacity of the ZnO based materials. However, several experiments are needed to further confirm the improved bioactivity of the core–shell nanoparticles.

Conflicts of interest

There are no conflicts to declare.

Acknowledgements

The authors wish to acknowledge the Fondecyt Incioacion 11160073 (KVP), Centro de Investigación de Polímeros Avanzados (CIPA), CONICYT Regional, and GORE BIO-BIO R17A10003. MMY acknowledge NIH for the funding support (R15-CA213232).

Notes and references

1 L. Wang, C. Hu and L. Shoa, *Int. J. Nanomed.*, 2017, **12**, 1227–1249.
2 Y. Shen, R. Zhuan, L. Chu, X. Xiang, H. Sun and J. Wang, *Waste Manag.*, 2019, **84**, 141–146.
3 K. Varaprasad, *Phosphorus, Sulfur Silicon Relat. Elem.*, 2018, **193**, 74–80.
4 K. Varaprasad, G. M. Raghavendra, T. Jayaramudu and J. Seo, *Carbohydr. Polym.*, 2016, **135**, 349–355.
5 F. P. Chen, B. S. Li and C. H. Tang, *J. Agric. Food Chem.*, 2015, **63**, 3559–3569.
6 Z. Zheng, X. Zhang, D. Carbo, C. Clark, C. A. Nathan and Y. Lvov, *Langmuir*, 2010, **26**, 7679–7681.
7 S. Agnihotri, G. Bajaj, S. Mukherji and S. Mukherji, *Nanoscale*, 2015, **7**, 7415–7429.
8 Y. W. Wang, A. Cao, Y. Jiang, X. Zhang, J. H. Liu, Y. Liu and H. Wang, *ACS Appl. Mater. Interfaces*, 2014, **6**, 2791–2798.
9 K. R. Raghupathi, R. T. Koodali and A. C. Manna, *Langmuir*, 2011, **27**, 4020–4028.
10 Y. J. Jo, E. Y. Choi, N. W. Choi and C. K. Kim, *Ind. Eng. Chem. Res.*, 2016, **55**, 7801–7809.
11 F. P. Chen, S. Y. Ou, Z. Chen and C. H. Tang, *J. Agric. Food Chem.*, 2017, **65**, 1707–1714.
12 P. Zou, L. Helson, A. Maitra, S. T. Stern and S. E. McNeil, *Mol. Pharm.*, 2013, **10**, 1977–1987.
13 I. R. Ariyarathna and D. N. Karunaratne, *Food Packaging Shelf*, 2016, **10**, 79–86.
14 B. Zheng, S. Peng, X. Zhang and D. J. McClements, *J. Agric. Food Chem.*, 2018, **66**, 10816–10826.
15 P. K. Singh, V. Kotia, D. Ghosh, G. M. Mohite, A. Kumar and S. K. Maji, *ACS Chem. Neurosci.*, 2013, **4**, 393–407.
16 R. K. B. Bhawana, H. S. Buttar, V. K. Jain and N. Jain, *J. Agric. Food Chem.*, 2011, **59**, 2056–2061.
17 T. Pal, S. Mohiyuddin and G. Packirisamy, *ACS Omega*, 2018, **3**, 831–843.
18 S. Govindaraju, A. Rengaraj, R. Arivazhagan, Y. S. Huh and K. Yun, *Bioconjugate Chem.*, 2018, **29**, 363–370.
19 S. B. Ghaffari, M. H. Sarrafzadeh, Z. Fakhroueian, S. Shahriari and M. R. Khorramizadeh, *Mater. Sci. Eng., C*, 2017, **79**, 465–472.
20 R. N. Moussawi and D. Patra, *RSC Adv.*, 2016, **6**, 17256–17268.
21 A. Rajasekar and T. Devasena, *J. Nanosci. Nanotechnol.*, 2015, **15**, 4119–4125.
22 C. Cheng, S. Peng, Z. Li, L. Zou, W. Liu and C. Liu, *RSC Adv.*, 2017, **7**, 25978–25986.
23 A. Kurniawan, F. Gunawan, A. T. Nugraha, S. Ismadji and M. J. Wang, *Int. J. Pharm.*, 2017, **516**, 158–169.
24 K. Varaprasad, K. Ramam, G. S. Mohan Reddy and R. Sadiku, *RSC Adv.*, 2014, **4**, 60363–60370.
25 B. Sun, Y. Tian, L. Chen and Z. Jin, *Food Hydrocolloids*, 2018, **77**, 911–920.
26 S. Raj and D. R. Shankaran, *Sens. Actuators, B*, 2016, **226**, 318–325.
27 R. Hariharan, S. Senthilkumar, A. Suganthi and M. Rajarajan, *Mater. Res. Bull.*, 2012, **47**, 3090–3099.
28 G. M. Raghavendra, T. Jayaramudu, K. Varaprasad, S. Ramesh and K. M. Raju, *RSC Adv.*, 2014, **4**, 3494–3501.
29 S. Buddee, S. Wongnawa, P. Sriprang and C. Sriwong, *J. Nanopart. Res.*, 2014, **16**, 2336.
30 H. Wang, X. Gong, X. Guo, C. Liu, Y. Y. Fan, J. Zhang, B. Niu and W. Li, *Int. J. Biol. Macromol.*, 2019, **121**, 1118–1125.
31 J. Yu, S. Zhuang, X. Xu, W. Zhu, B. Feng and J. Hu, *J. Mater. Chem. A*, 2015, **3**, 1199–1207.
32 J. Chen, C. Ning, Z. Zhou, P. Yu, Y. Zhu, G. Tan and C. Mao, *Prog. Mater. Sci.*, 2019, **99**, 1–26.
33 X. P. Li, Y. L. Sun, C. W. Luo and Z. S. Chao, *Ceram. Int.*, 2018, **44**, 13439–13443.
34 S. Bisht, G. Feldmann, S. Soni, R. Ravi, C. Karikar, A. Maitra and A. Maitra, *J. Nanobiotechnol.*, 2007, **5**, 1–18.
35 E. G. Goh, X. Xu and P. G. McCormick, *Scr. Mater.*, 2014, **78–79**, 49–52.
36 B. Jin, P. Zheng, W. Guan, B. Bai, B. Zhang and S. Dai, *ChemNanoMat*, 2018, **4**, 972–981.
37 F. Noreen, A. Iqbal, G. Hussain, S. Kanwal and S. A. Khan, *Mater. Sci. Eng., C*, 2017, **82**, 46–59.
38 C. T. Ng, L. Q. Yong, M. P. Hande, C. N. Ong, L. Yu, B. H. Bay and G. H. Baeg, *Int. J. Nanomed.*, 2017, **12**, 1621–1637.
39 D. Setyaningsih, Y. B. Murti, S. Martono, W. L. J. Hinrichs, T. Hertiani and A. Fudholi, *Int. J. Pharm. Clin. Res.*, 2016, **8**, 377–386.

